Check for updates

Received: 18 May 2021 | Accepted: 27 June 2021

DOI: 10.1002/iub.2528

SPECIAL ISSUE

IUBMB LIFE WILEY

Condition-dependent structural collapse in the intrinsically disordered N-terminal domain of prion protein

Eric H.-L. Chen[1] | **Kuei-Ming Lin**[1,2] | **Jason C. Sang**[1] | **Meng-Ru Ho**[1] | **Chih-Hsuan Lee**[1,2] | **Orion Shih**[3] | **Chun-Jen Su**[3] | **Yi-Qi Yeh**[3] | **U-Ser Jeng**[3,4] | **Rita P.-Y. Chen**[1,2,5]

[1]Institute of Biological Chemistry, Academia Sinica, Taipei, Taiwan

[2]Institute of Biochemical Sciences, National Taiwan University, Taipei, Taiwan

[3]National Synchrotron Radiation Research Center, Hsinchu, Taiwan

[4]Department of Chemical Engineering, National Tsing Hua University, Hsinchu, Taiwan

[5]Neuroscience Program of Academia Sinica, Academia Sinica, Taipei, Taiwan

Correspondence
Rita P.-Y. Chen, Institute of Biological Chemistry, Academia Sinica, No. 128, Sec. 2, Academia Rd., Nankang, Taipei, 115, Taiwan.
Email: pyc@gate.sinica.edu.tw

Funding information
Academia Sinica

Abstract

Prion protein is composed of a structure-unsolved N-terminal domain and a globular C-terminal domain. Under limited trypsin digestion, mouse recombinant prion protein can be cleaved into two parts at residue Lys105. Here, we termed these two fragments as the N-domain (sequence 23–105) and the C-domain (sequence 106–230). In this study, the structural properties of the N-domain, the C-domain, and the full-length protein were explored using small-angle X-ray scattering, analytical ultracentrifugation, circular dichroism spectroscopy, and the 8-anilino-1-naphthalenesulfonic acid binding assay. The conformation and size of the prion protein were found to change sensitively under the solvent conditions. The positive residues in the sequence 23–99 of the N-domain were found to be responsible for the enhanced flexibility with the salt concentration reduced below 5 mM. The C-domain containing a hydrophobic patch tends to unfold and aggregate during a salt-induced structural collapse. The N-domain collapsed together with the C-domain at pH 5.2, whereas it collapsed independently at pH 4.2. The positively charged cluster (sequence 100–105) in the N-domain contributed to protecting the exposed hydrophobic surface of the C-domain.

KEYWORDS

intrinsically disordered, N-terminal, prion, structural collapse

Abbreviations: Aβ, amyloid-β peptide; AcOH, acetic acid; AD, Alzheimer's disease; ANS, 8-anilino-1-naphthalenesulfonic acid; Bis-Tris, bis(2-hydroxyethyl)amino-tris(hydroxymethyl)methane; CD, circular dichroism; EOM, ensemble optimization method; ESI, electrospray ionization; FL-mPrP, full-length recombinant mouse prion protein; HPLC, high performance liquid chromatography; HR, hydrophobic region; IMAC, immobilized metal affinity chromatography; MALD, matrix-assisted laser desorption ionization; NaOAc, sodium acetate; OD, optical density; OR, octapeptide repeat; PMSF, phenylmethylsulfonyl fluoride; PCC, positively charged cluster; *PRNP*, prion protein gene; PrP, prion protein; PrP^{C}, normal/cellular form of prion protein; PrP^{Sc}, scrapie/disease form of prion protein; PrP^{sen}, protease-sensitive form of prion protein; PrP^{res}, protease-resistant form of prion protein; R_g, radius of gyration; R_h, hydrodynamic radius; SAXS, small-angle X-ray scattering; SDS-PAGE, sodium dodecyl sulfate polyacrylamide gel electrophoresis; SV-AUC, sedimentation velocity-analytical ultracentrifugation; T_m, melting temperature; TOF, time-of-flight; UV, ultraviolet.

 © 2021 International Union of Biochemistry and Molecular Biology.

1 | INTRODUCTION

Prion diseases are special types of neurodegenerative diseases that manifest in a sporadic, inherited, and transmissible manner. The infectious material was named prion by Prof. Stanley B. Prusiner.[1,2] Prion is composed of protein aggregates formed from misfolded cellular prion protein (PrP^C). PrP^C is a glycosylphosphatidylinositol-anchored membrane protein situated on the outer membrane of neuron cells. Its N-terminal sequence 1–22 and C-terminal sequence 231–254 are the signal peptides and cleaved during protein translocation. It has a globular structure at its C-terminus, but its N-terminal part (sequence 23–110) is unstructured.[3] In the prion pathogenesis, PrP^C is converted to a misfolded form named PrP^{Sc}, and PrP^{Sc} tends to self-association and forms prion. The structural conversion from PrP^C to PrP^{Sc} occurs at the C-terminal globular domain,[4–12] and the N-terminal unstructured segment is protease-sensitive and can be removed from PrP^{Sc} without affecting its infectivity. Therefore, the unstructured N-terminal segment has received less attention than the C-terminal globular domain in studies on prion.

The role of the N-terminal segment in the structure and function of PrP^C and prion conversion is not yet clear. It has been proposed that the N-terminal segment of PrP^C could be a receptor of Aβ oligomers in the toxic signaling pathway and that PrP^C could be a potential therapeutic target of Alzheimer's disease (AD).[13,14] PrP^C-Aβ binding can be seen in AD patients but not in normal controls.[15] Lauren et al. reported that soluble amyloid-β oligomers block hippocampal long-term potentiation. In contrast, the same phenomenon did not occur in the hippocampal slices of PrP-null mice.[16] The authors identified PrP^C as an Aβ oligomer receptor with a dissociation constant of 92 nM. Using various deletion mutants and anti-PrP antibodies, they concluded that the 95–105 region (sequence HNQWNKPSKPK) is the principal site for Aβ42-oligomer binding. Using the surface plasmon resonance technique, Chen et al. reported an additional Aβ oligomer binding site at the extreme amino-terminus (sequence 23–27, KKRPK).[17] Both sites (23–27 and 95–105) contain a cluster of polybasic residues.

Recent research has shown that these polybasic segments are crucial for prion pathogenesis. Mice devoid of PrP were resistant to prion infection,[18] and the introduction of the *PRNP* gene or the N-terminal truncated (Δ32–80, Δ32–93) *PRNP* gene restored prion susceptibility.[19,20] The $PrP^{0/0}$ mice expressing PrP with Lys-23, Lys-24, and Lys-27 mutated to Ala reduced susceptibility to prion infection.[21] It has also been reported that haPrPΔ34–113 altered PrP^{res} conformation and haPrPΔ34–94 did not[22] ("ha" stands for hamster and "res" stands for resistant). These findings indicate that these basic residues in the N-terminal region (in the regions 23–27 and 95–105) might be related to the interaction between PrP^C and PrP^{Sc} or might be important in the structural conversion of PrP^C.

In contrast to the finding that $PrP^{0/0}$ mice expressing mPrPΔ32–80, mPrPΔ32–93, mPrPΔ32–106, and mPrPΔ114–121 transgenes are healthy, $PrP^{0/0}$ mice expressing mPrPΔ32–121, mPrPΔ32–134, mPrPΔ94–134, and mPrPΔ105–125 spontaneously developed severe neurodegeneration.[23–26] This deletion-induced neurotoxic effect can be abrogated by the coexpression of full-length PrP (except for mPrPΔ105–125). PrP with the deletion of 105–125 is particularly toxic and leads to animal death within 1 week.[25,27,28] The data obtained from these N-terminal deletions imply the protective role of the sequence 105–113 in the toxicity caused by those PrP deletion mutants.[26]

In this study, we found that full-length recombinant mouse prion protein (denoted as FL-mPrP) can be separated into two domains—called the N-domain and the C-domain in this study—by mild trypsin digestion. The N-domain encompasses sequence 23–105, and the C-domain encompasses sequence 106–230. The structural properties of these two domains were characterized by biophysical methods to clarify the effect of the N-domain on the full-length protein.

2 | EXPERIMENTAL PROCEDURES

2.1 | Expression and purification of FL-mPrP, the N-domain, and the C-domain

The genes corresponding to mouse PrP sequences 23–230, 23–105, and 106–230 with codon optimization (GenScript, NJ, USA) were cloned into pET28a. The translated full-length mPrP(23–230) was encoded FL-mPrP. FL-mPrP had 209 residues, corresponding to mouse prion sequence 23–230 plus an extra Gly at its N-terminus. The Met residue coded by the initiation codon was cleaved by methionine aminopeptidase in *Escherichia coli*.[29,30] The N-domain contains mouse prion protein 23–105 plus an extra Gly at its N-terminus with a molecular mass of 8.6 kDa. The C-domain contains mouse prion protein 106–230 with a molecular mass of 14.5 kDa.

The plasmids were transformed into *E. coli* BL21 Star (DE3) (Invitrogen, CA, USA). To express proteins, an overnight culture was used to inoculate fresh Luria-Bertani medium containing kanamycin (50 μg/ml), and the cells were grown at 37°C by vigorous shaking (250 rpm) until $O.D._{600}$ reached 0.6. Protein expression was induced by

adding isopropyl β-D-1-thiogalactopyranoside to a final concentration of 1 mM, and the culture was grown for an additional 5 hr. The cells were then harvested by centrifugation at 3,000*g* at 4°C for 15 min. The cell pellet was resuspended in the cell lysis buffer (50 mM Tris, 100 mM NaCl, and pH 8.0 at about 9 ml/g cell), and cell lysis was conducted by incubating with 0.1 × CelLytic B, 0.15 mg/ml lysozyme, 25 μg/ml DNaseI, 7 mM $MgCl_2$, and 1 mM phenylmethylsulfonyl fluoride (PMSF) for 30 min at room temperature by stirring.

FL-mPrP, the N-domain, and the C-domain formed inclusion bodies in *E. coli*. Inclusion bodies were collected from the cell lysate by centrifugation at 20,000*g* for 30 min at 4°C and resuspended in the immobilized metal affinity chromatography (IMAC) buffer A (8 M urea, 100 mM Na_2HPO_4, 10 mM Tris–HCl, pH 8.0). The suspended solution was rotated at 40 rpm for 2 hr at 4°C and then centrifuged at 30,000*g* for 30 min at 4°C. For FL-mPrP, the supernatant containing the solubilized proteins was collected and filtered through a 0.45 μM Millipore syringe filter and loaded onto the nickel-chelating Sepharose column (GE Healthcare, IL, USA). After washing with five column volumes of the IMAC buffer A, FL-mPrP was eluted with IMAC buffer B (8 M urea, 100 mM Na_2HPO_4, 10 mM Tris–HCl, and 20 mM ethylenediaminetetraacetic acid [EDTA]). The eluted FL-mPrP was further purified by reverse-phase high-pressure liquid chromatography (HPLC) on a C5 column (Discovery BIO Wide Pore C5, 10 μm, 250 mm × 10 mm, Supelco, USA). S11 can be purified by the same protocol. The production yield is lower because the binding ability of S11 to the nickel-chelating Sepharose column is lower.

For the N-domain and the C-domain, the supernatant containing the solubilized proteins from inclusion bodies was filtered through a 0.45-μM Millipore syringe filter and loaded onto a prepacked HiLoad 16/60 Superdex 200 column (GE Healthcare, IL, USA) pre-equilibrated with the IMAC buffer A. The target protein was collected and further purified by HPLC as described earlier.

Protein identification was examined by electrospray ionization time-of-flight (ESI-TOF) mass spectrometry. The eluted protein was lyophilized and stored at −30°C.

2.2 | Trypsin digestion assay

FL-mPrP was dissolved in 0.5 mM NaOAc (pH 7) to make a solution (0.8 mg/ml). Trypsin (Sigma, USA) was added to the protein solution. The final protein concentration was 0.4 mg/ml, and the final trypsin concentration was 0, 5, 25, or 50 μg/ml. The digestion was conducted at 37°C for 1 hr and then stopped by adding PMSF (1 mM). The digested product was analyzed on 12% Bis-Tris gel by sodium dodecyl sulfate polyacrylamide gel electrophoresis (SDS-PAGE).

2.3 | Sedimentation velocity-analytical ultracentrifugation

The sedimentation velocity-analytical ultracentrifugation (SV-AUC) experiments were performed using an XL-A analytical ultracentrifuge (Beckman Coulter, USA) equipped with an An-60 Ti rotor (Beckman Coulter, USA). Proteins were dissolved in the indicated solution at a concentration of 10 μM (230 μg/ml), loaded into a two-sector centerpiece (12-mm, charcoal-filled epon) and centrifuged at 20°C at a speed of 201,060*g* (50,000 rpm) for 16 hr. The absorbance of the samples at 280 nm was monitored in a continuous mode at time intervals of 5 min. The partial specific volume ($\bar{\nu}$), buffer density, and viscosity were calculated by SEDNTERP.[31] Data were analyzed with the standard c(s) method in SEDFIT 13.36,[32] and the continuous c(s) distribution was plotted using OriginLab.

2.4 | Circular dichroism spectroscopy

Proteins were dissolved in the indicated solution to a final concentration of 10 μM and then placed in a quartz cell with a 1-mm path length. The circular dichroism (CD) spectra between 190 and 250 nm were recorded on a J-815 CD spectrometer (JASCO, Japan). The band width was set to 2 nm, and the step resolution was 0.05 nm. Two scans were averaged for each sample. Thermal stability was measured by increasing temperature from 25 to 95°C (1°C increment followed by a 2-min equilibration period). The observation wavelength was 222 nm. The thermal denaturation curves were fitted using the equation of the two-state model.

2.5 | ANS-binding assay

ANS (8-anilino-1-naphthalenesulfonic acid) is a small molecule dye composed of a sulfonated naphthalene and an anilino group. ANS is amphipathic, and its fluorescence quantum yield increases dramatically when the dye binds to a hydrophobic region of a protein. Proteins were dissolved in the indicated solvent and the ANS solution was added. The final protein concentration was 10 μM. The molar ratio of protein to ANS was 1–180. Excited at 380 nm, the fluorescence emission spectrum of the protein/ANS mixture was recorded

between 400 and 650 nm on a Fluorolog-3 (Horiba, Japan). The slit for excitation and emission was set to 1 nm. Six scans were averaged to get the final spectrum for each sample.

2.6 | Small-angle X-ray scattering

FL-mPrP was dissolved in 0.5 mM acetic acid (AcOH) (pH 4.2) and centrifuged at 14,000 rpm for 15 min to remove precipitates. The protein concentration used for small-angle X-ray scattering (SAXS) was 0.5 mg/ml as quantitated by UV absorption. SAXS data were collected using the BL23A SAXS beamline at the Taiwan Light Source of National Synchrotron Radiation Research Center in Hsinchu, using a monochromatic 15 keV X-ray beam ($\lambda = 0.828$ Å) of 0.5 mm diameter. The instrument is equipped with a sample flow-purification system incorporated with an HPLC system (Agilent chromatographic system 1260 series).[33,34] The column-bypass flow mode of the system was used because of the unwanted strong interaction between FL-mPrP and silica gel inside the size exclusion column, which would lead to sample entrapment inside the column. SAXS data were collected (30 s/frame for 10 frames) during the sample flow (0.2 ml/min) within a thin-wall (30 μm) quartz capillary cell (2.0 mm diameter) thermostated at 288 K. The sample-to-detector distance of 2.52 m together with a Pilatus 1M-F area detector covered a reasonable scattering vector q-range, where $q = 4\pi\lambda^{-1}\sin\theta$ is defined by the scattering angle 2θ and λ.

3 | RESULTS

3.1 | Mouse PrP can be separated into the N-domain and the C-domain by trypsin digestion

The structure of PrP was commonly depicted as a globular domain plus an unstructured, flexible linear chain. When trypsin digestion was employed to examine the structural integrity of mouse PrP, we found that FL-mPrP can be cut into two fragments, shown as two bands on the gel of SDS-PAGE in Figure 1a. These two fragments were separated by a C18 column and HPLC and analyzed by ESI mass spectrometry (Figure S1). The upper band near 15 kD corresponded to the C-terminal fragment with sequence 106–230 (encoded as the C-domain here). The lower band of ~12–13 kD was the N-terminal fragment containing the residues 23–105 (encoded as the N-domain here). The lower band is situated at a position higher than it should be because the N-domain is intrinsically disordered and has a lower content of hydrophobic residues to bind SDS. The mass data indicated that the trypsin cutting site is located at Lys105-Thr106. The potential trypsin cutting sites are shown in Figure 1b. There are nine trypsin cutting sites (6K, 3R) in the sequence of 23–105 and 13 trypsin cutting sites (5K, 8R) in 106–230. Lys105 is the first cutting site, implying that the N-domain might not be as flexible and solvent-accessible as we thought, and residue-105 is in the hinge region between the N-domain and the C-domain. In the N-domain, there is a long octarepeat sequence without

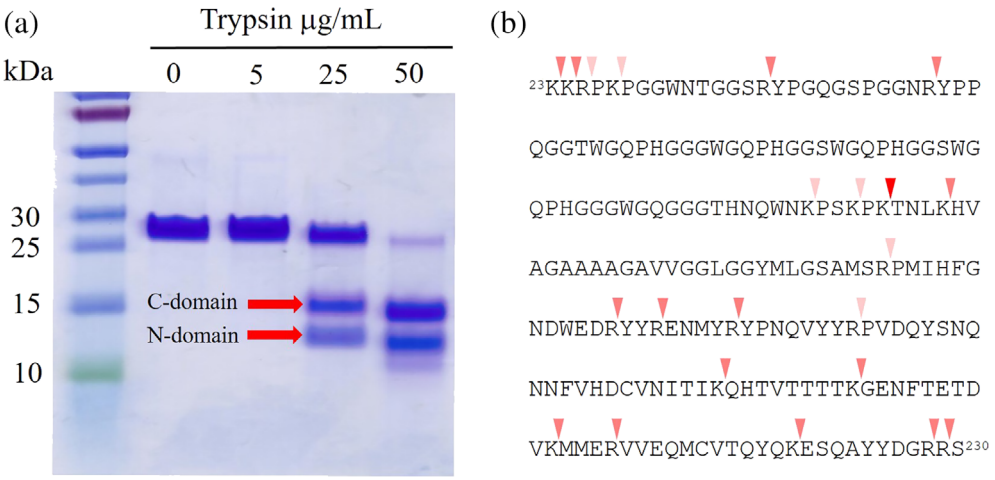

FIGURE 1 (a) The SDS-PAGE of FL-mPrP after trypsin digestion. The protein was dissolved in 0.5 mM NaOAc (pH 7) and digested by different concentrations of trypsin at 37°C for 1 hr. (b) Amino acid sequence of the mouse prion protein. The trypsin cutting sites are marked with arrows. The dark red arrow is the cutting site K105-T106 separating the N-domain and the C-domain. The pink arrows indicate the potential trypsin cutting sites. The light pink arrows indicate the K–P and R–P sequences, which have lower trypsin cutting frequency.[35] FL-mPrP, full-length recombinant mouse prion protein; SDS-PAGE, sodium dodecyl sulfate polyacrylamide gel electrophoresis

any trypsin digestion site in the middle region. Moreover, there are four K–P and R–P sequences in the N-domain, which have lower frequencies in trypsin digestion.[35] Because trypsin cuts at the C-terminal site of Lys or Arg, the polybasic sites (23–27 and 95–105) are also the clusters of trypsin cutting sites. The fact that Lys105 is the first cutting site also implies that these two polybasic regions might interact with other parts of the protein at neutral pH.

3.2 | Solvent-dependent structural mobility and compactness of FL-mPrP

Figure 2a shows the SAXS data of FL-mPrP dissolved in 0.5 mM AcOH (pH 4.2). The Guinier approximation of the SAXS data shows multiple slopes, representing polydispersity in radius of gyration (R_g). Therefore, the SAXS data were fitted using the ensemble optimization method (EOM)[36,37] to describe the polymorphism behavior of the protein. EOM fits the data using an ensemble of conformations, which is a pool of independent structural models. In this case, the pool contains fully flexible chains and partially flexible chains that have a rigid C-domain reported previously (PDB ID: 2L1H) to cover wider possibilities. The R_g distribution of the structural pool is shown in Figure 2b. The fitting protocol searched possible combinations from the pools to fit the data and evaluated the fitting quality based on the χ^2 value. The ensemble that best describes the experimental SAXS data (Figure 2a) has nine models, of equal probability, distributed into two groups: G1 (67% population) and G2 (33% population); their corresponding R_g values are marked in Figure 2b. G1 contains six models reconstructed with a rigid C-domain reported previously (PDB ID: 2L1H), leaving the N-domain flexible, as shown in Figure 2c; the three conformations in G2 are reconstructed with no restriction on the C-domain (Figure 2d–f). The best-fitted model combination reflects the key features of the protein polymorphism. We note that the average R_g value 40.5 ± 0.99 Å of this best-fitted ensemble is significantly larger than 30.5 Å reported observed previously by Carter et al. in 2015.[38] In Carter's study, FL-mPrP was dissolved in 20 mM NaOAc/150 mM NaCl (pH 5.1). Because FL-mPrP is prone to aggregation at their solvent condition,[38] we chose a different buffer of 0.5 mM AcOH (pH 4.2) to increase solubility. The significantly larger protein conformations observed from SAXS might result from the

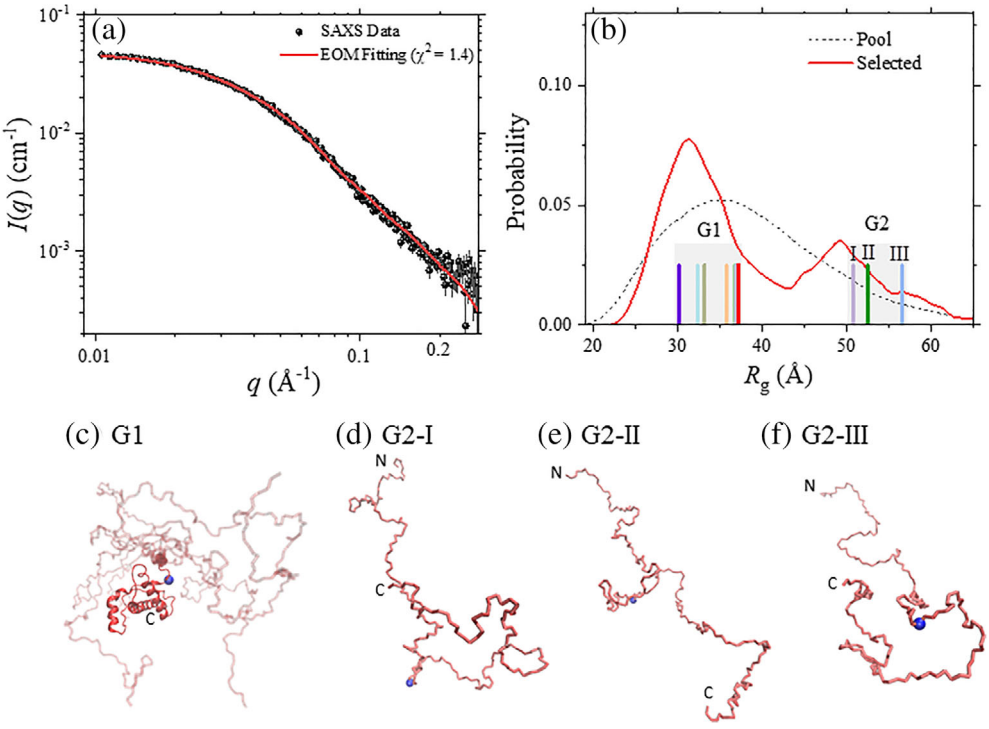

FIGURE 2 (a) SAXS data of FL-mPrP in 0.5 mM AcOH (pH 4.2). The data are fitted (solid curve) using EOM with an optimal ensemble of nine models. (b) Comparison of the R_g distribution of the EOM generated pool (black dotted line) and the selected model ensemble (red line). The R_g values of the optimal ensemble were divided into two groups: G1 and G2. (c) The six reconstructed models in the G1 group with the same C-domain overlapped. (d–f) The reconstructed models in the G2 group. The trypsin cleavage site at K105-T106 is marked with a blue dot. AcOH, acetic acid; EOM, ensemble optimization method; FL-mPrP, full-length recombinant mouse prion protein; SAXS, small-angle X-ray scattering

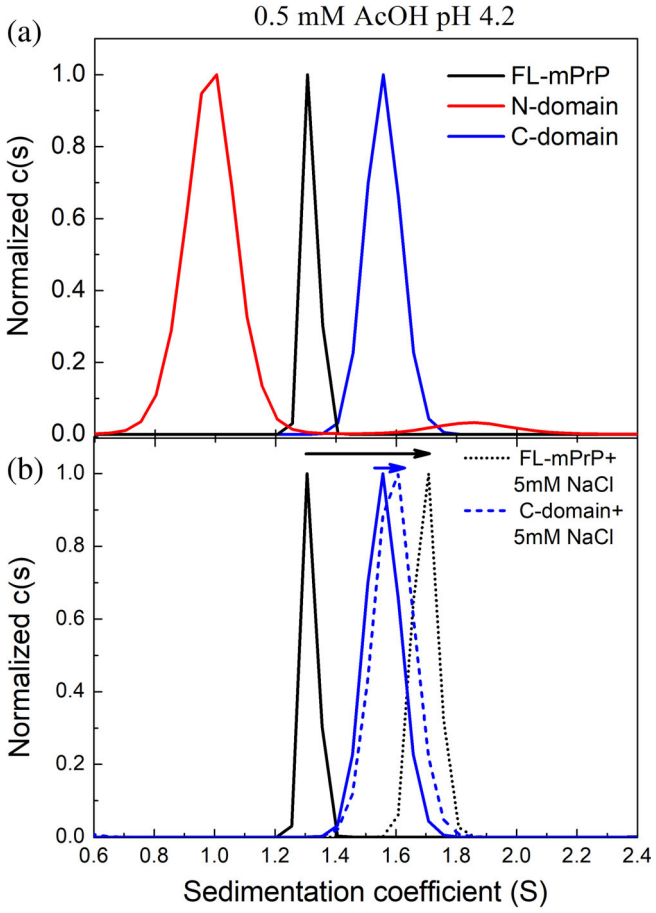

FIGURE 3 The SV-AUC spectra of FL-mPrP, the N-domain, and the C-domain. (a) The proteins were dissolved in 0.5 mM AcOH (pH 4.2). (b) The sedimentation coefficient changes of FL-mPrP and the C-domain with the addition of NaCl. Black: FL-mPrP; red: N-domain; blue: C-domain. Solid line: without NaCl; dashed line: with NaCl. The sedimentation coefficient change with the addition of NaCl is marked with arrows in (b). AcOH, acetic acid; FL-mPrP, full-length recombinant mouse prion protein; SV-AUC, sedimentation velocity-analytical ultracentrifugation

relaxation of the salt and pH-sensitive interactions between the N-domain and C-domain consequently.

Therefore, FL-mPrP, the N-domain, and the C-domain were dissolved in 0.5 mM AcOH and analyzed using analytical ultracentrifugation (AUC) (Figure 3a). Unexpectedly, the sedimentation coefficient is C-domain > FL-mPrP > N-domain. FL-mPrP has a sedimentation coefficient lower than its C-terminal fragment, indicating that the N-terminal part of FL-mPrP in 0.5 mM AcOH (pH 4.2) is flexible, and this flexible region increases the friction during sedimentation. When 5 mM NaCl was added to the solution, the sedimentation coefficient of FL-mPrP increased from 1.32 ± 0.15 S to 1.72 ± 0.08 S, corresponding to the hydrodynamic radius (R_h) that decreased from 4.07 ± 0.12 nm to 3.13 ± 0.10 nm (Figure 3b, Table 1). On the contrary, the sedimentation of the C-domain was not affected by the addition of salt (Figure 3b). These data suggest that ionic strength induced the structural collapse of the N-domain.

The structural collapse of the N-domain was further supported by the ANS-binding assay. ANS is a dye with the fluorescence quantum yield of which is greatly increased when it binds to clustered and exposed regions of hydrophobicity on a protein. As shown in Figure 4, the fluorescence intensities of FL-mPrP and the N-domain were largely reduced in the presence of 5 mM NaCl. This indicates that 5 mM salt was enough to induce the hydrophobic collapse of the N-domain region in full-length protein, and the hydrophobic surface was buried in the collapsed structure. However, the C-domain's fluorescence intensity in the presence of 5 mM NaCl increased substantially. The data imply that the C-domain exposed a more hydrophobic surface in the presence of salt. This explains why the C-domain has lower solubility in a high-salt solution and is prone to aggregation.

3.3 | Structural collapse of the N-domain does not affect the structural stability of the C-domain at pH lower than 5

CD spectroscopy is a useful technique to measure secondary structure change. The C-domain has three long α-helices and two short β-strands. Both CD spectra of FL-mPrP and of the C-domain showed a clear α-helical structural feature (strong positive peak at ~192 nm and two negative peaks at ~208 and 222 nm) (Figure S2). The structural stability of FL-mPrP and the C-domain was measured by thermal denaturation using CD spectroscopy. With the increase of temperature, the spectra showed a clear two-phase transition from the helix-rich spectrum to the random coil-rich spectrum (negative peak at ~200 nm) with an isodichroic point at 205 nm (Figure 5a,b). The same melting temperatures could be obtained either by using the ellipticity at 222 nm, the wavelength corresponding to the structured region of the protein, or the ellipticity at 200 nm, the wavelength corresponding to the unstructured region of the protein, to plot the thermal denaturation curves, proving the protein undergoes cooperative unfolding/refolding (Figure S3). The melting temperature of FL-mPrP and the C-domain in 0.5 mM AcOH is 62.5 ± 0.7°C and 62.0 ± 0.5°C, respectively, indicating that the flexible N-domain did not affect the structural stability of the C-domain (Figure 5c,d). With the addition of 5 mM NaCl, the melting temperature of FL-mPrP and the C-domain is 62.0 ± 0.9°C and 62.6 ± 0.4°C, respectively (Figure 5e,f). This result suggests that the N-domain collapse upon

TABLE 1 The melting temperature and size obtained in this study for FL-mPrP and the C-domain

pH 4.2	FL-mPrP, 0.5 mM, AcOH	FL-mPrP, 0.5 mM AcOH, +5 mM NaCl	C-domain, 0.5 mM AcOH	C-domain, 0.5 mM AcOH, +5 mM NaCl
Sedimentation coefficient (S)	1.32 ± 0.15	1.72 ± 0.08	1.55 ± 0.08	1.6 ± 0.07
R_h (nm), (AUC)	4.07 ± 0.12	3.13 ± 0.10	2.18 ± 0.10	2.11 ± 0.08
T_m (°C)	62.5 ± 0.7	62.0 ± 0.9	62.0 ± 0.5	62.6 ± 0.4
R_g[a] (nm), (SAXS)	4.05 ± 0.99	–	–	–
pH 5.2	**FL-mPrP, 0.5 mM, NaOAc**	**FL-mPrP, 5 mM NaOAc**	**FL-mPrP, 20 mM NaOAc**	**C-domain, 0.5 mM NaOAc**
Sedimentation coefficient (S)	1.62 ± 0.05	1.86 ± 0.09	1.90 ± 0.12	–
R_h (nm), (AUC)	3.32 ± 0.10	2.89 ± 0.16	2.83 ± 0.19	–
T_m (°C)	67.8 ± 0.8	70.3 ± 0.5	69.3 ± 0.6	69.4 ± 0.8

Note: "–": data not available.

Abbreviations: AcOH, acetic acid; AUC, analytical ultracentrifugation; FL-mPrP, full-length recombinant mouse prion protein; SAXS, small-angle X-ray scattering.

[a]Ensemble average from the nine model R_g values shown in Figure 2b; the large uncertainty of R_g reflects protein polymorphism.

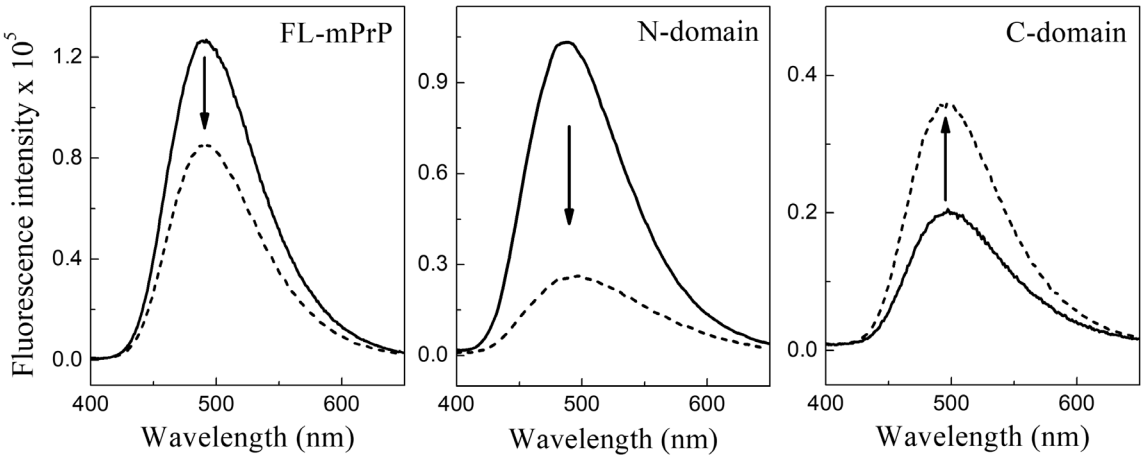

FIGURE 4 The fluorescence spectra of FL-mPrP, the N-domain, and the C-domain after ANS binding. Proteins were dissolved in 0.5 mM AcOH (pH 4.2) with or without 5 mM NaCl. Solid line: without NaCl; dashed line: with NaCl. The spectral change upon salt increase is indicated by an arrow. AcOH, acetic acid; ANS, 8-anilino-1-naphthalenesulfonic acid; FL-mPrP, full-length recombinant mouse prion protein

increasing the salt did not affect the C-domain structural stability.

3.4 | Structural compactness of FL-mPrP is pH-sensitive

At pH 4.2, the existence of the N-domain and the salt-induced structural collapse of the N-domain did not affect the structural stability of the C-domain. Because 4.2 is lower than the pKa of Glu, the absence of interaction between these two domains might be due to the protonation of Glu. When FL-mPrP was dissolved in 0.5 mM NaOAc (pH 5.2), the AUC data suggested that FL-mPrP became more compact than in 0.5 mM AcOH (pH 4.2). In Figure 6a, the sedimentation coefficient of FL-mPrP is 1.62 ± 0.05 S at pH 5.2 compared with 1.32 ± 0.15 S at pH 4.2. Increasing ionic strength from 0.5 to 5 mM NaOAc at pH 5.2 also increased the sedimentation coefficient from 1.62 ± 0.05 S to 1.86 ± 0.09 S, corresponding to the hydrodynamic radius change from 3.32 ± 0.10 nm to 2.89 ± 0.16 nm (Table 1). Increasing salt concentration to 20 mM did not further enhance the effect.

The reduced fluorescence intensity in the ANS-binding assay in Figure 6b also indicated a reduced hydrophobic surface, which resulted from the

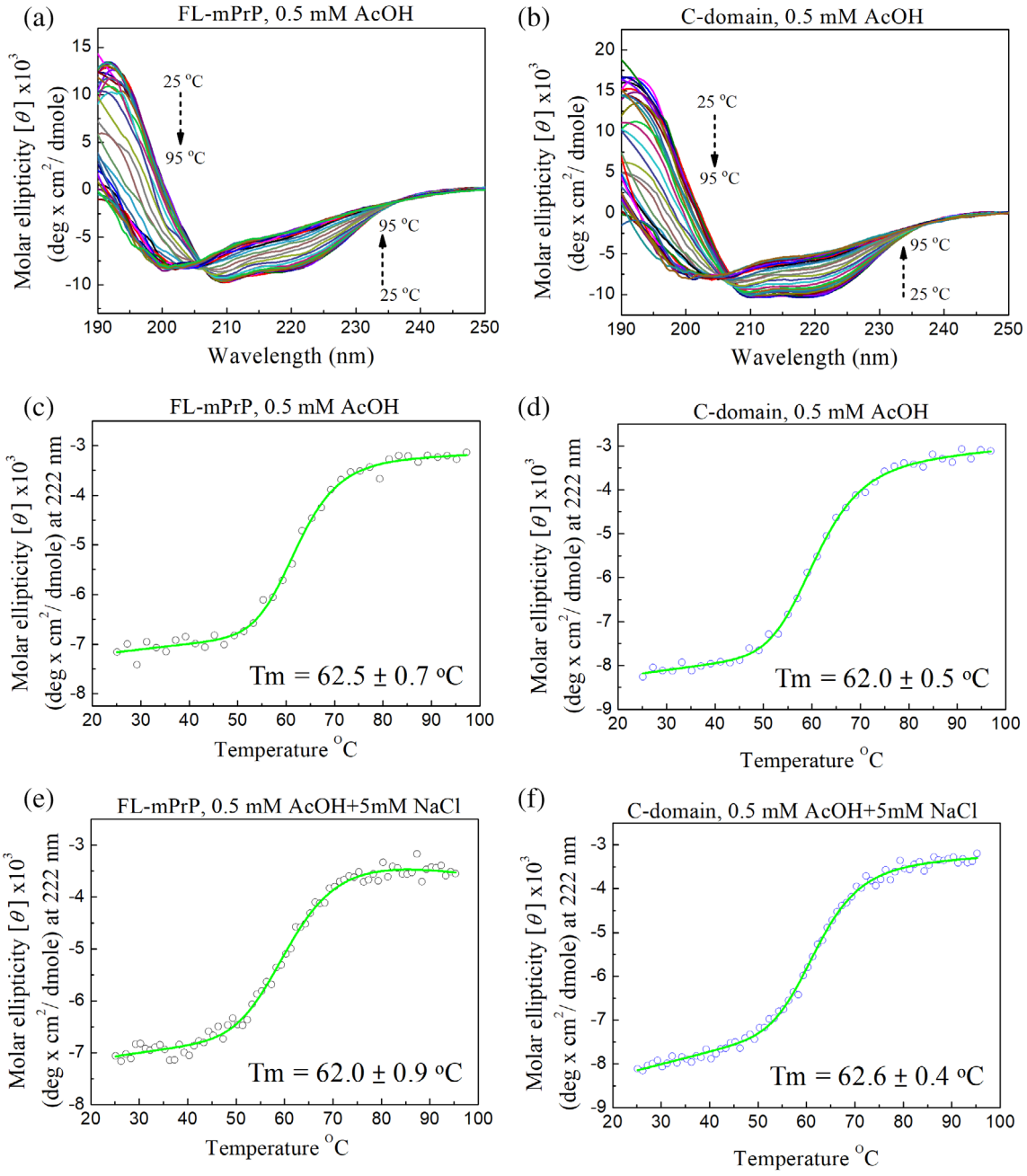

FIGURE 5 The thermal denaturation of FL-mPrP and the C-domain in 0.5 mM AcOH (pH 4.2) with or without 5 mM NaCl. (a,b) CD spectra of FL-mPrP and the C-domain in 0.5 mM AcOH (pH 4.2) at a temperature from 25 to 95°C. The direction of spectral change upon temperature increase is indicated by arrows. (c–f) The thermal denaturation curves of FL-mPrP (c,e) and the C-domain (d,f) in 0.5 mM AcOH (pH 4.2) with or without 5 mM NaCl. The melting temperature (T_m) of the sample is shown in each plot. AcOH, acetic acid; CD, circular dichroism; FL-mPrP, full-length recombinant mouse prion protein

hydrophobic collapse of this protein. Similar to the data obtained at pH 4.2, the structural collapse of mPrP at pH 5.2 was also sensitive to the small salt concentration increase. The melting temperatures of both FL-mPrP and the C-domain increased from 63 to ~69°C when the pH value increased from 4.2 to 5.2 (Figure 7). The difference in structural stability between the pH higher and lower than 5 indicates that the increase of stability might be due to the ionic interaction between positively charged residues and the Glu residues. The fact that the sedimentation coefficient of FL-mPrP was affected by the pH change suggests that the electrostatic interaction between the positively charged residues in the N-domain and the Glu residues in the C-domain

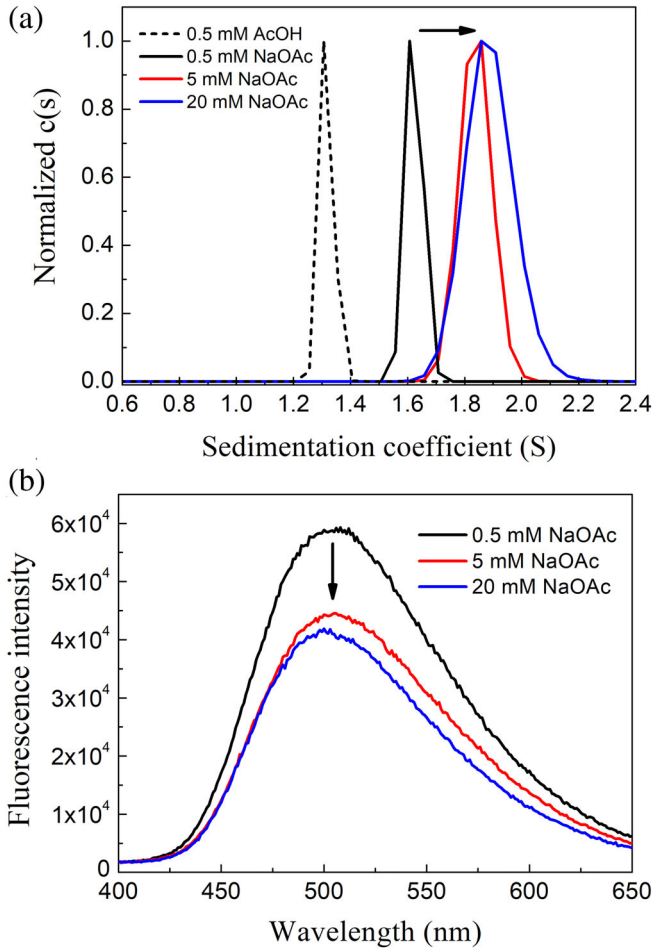

FIGURE 6 The SV-AUC spectra of FL-mPrP (a) and the fluorescence spectra of FL-mPrP after ANS binding (b) at different pH values and salt concentrations. FL-mPrP was dissolved in 0.5 mM AcOH (pH 4.2) (black dashed line), 0.5 mM NaOAc (pH 5.2) (black solid line), 5 mM NaOAc (pH 5.2) (red solid line), or 20 mM NaOAc (pH 5.2) (blue solid line). The protein concentrations of the samples are the same, as quantitated by UV absorption. The spectral change upon salt increase is indicated by an arrow. AcOH, acetic acid; ANS, 8-anilino-1-naphthalenesulfonic acid; FL-mPrP, full-length recombinant mouse prion protein; SV-AUC, sedimentation velocity-analytical ultracentrifugation

contributed to the structural collapse of FL-mPrP at pH higher than 5. However, the interaction only occurred on the protein surface and did not affect the secondary structures of the C-domain.

The salt-dependent experiment could not be done for the C-domain at pH 5.2 because the C-domain aggregated when the NaOAc concentration increased. Moreover, because most of the tryptophan residues exist in the N-domain, a higher concentration would be required to detect the C-domain in the AUC experiment. The C-domain cannot remain in the monomeric form at high protein concentrations.

3.5 | The flexibility of the N-domain relies on the positively charged residues in 23–99

Ahead of the positively charged cluster (PCC; sequence 100–105; KPSKPK), the region of 23–99 contains 3 Lys, 3 Arg, and 5 His. We mutated these 11 residues to serine, and the resulting mutant protein was named S11. The AUC results of S11 show that S11 is more compact than the wild-type protein FL-mPrP in the same solvent condition (Figure 8). The sedimentation coefficient of S11 in 0.5 mM AcOH is 1.76 ± 0.05 S compared with 1.32 ± 0.15 S of FL-mPrP (Table S1), suggesting that the 11 positively charged residues are important for the flexibility of the PrP N-terminal segment. The melting temperature of S11 in 0.5 mM AcOH (pH 4.2) and 0.5 mM NaOAc (pH 5.2) is 62.3 ± 0.5 and 68.5 ± 0.7°C, respectively, very close to the value of FL-mPrP in the same solvent (Figure S4). This further confirms that the positively charged residues in the PrP N-terminal part do not affect the structural stability of the PrP C-terminal globular domain.

4 | DISCUSSION

In this study, we disclosed how the solvent condition affects the size and stability of the full-length mouse prion protein. The structural collapse of prion protein was salt- and pH-dependent, and the major difference occurred in the N-terminal intrinsically disordered region. Our data are summarized in Table 1 and compared in Figure 9a. The salt-induced hydrophobic collapse in the N-terminal part of FL-mPrP was especially sensitive at low salt concentrations. The N-terminal part of prion protein had a loosely packed coil structure only when the protein was dissolved in water or a mild acidic condition (pH 4.2) without salt (Figure 3 and Figure S5). In those conditions, the N-terminal "flexible" polypeptide chain of FL-mPrP led to an unusually low sedimentation coefficient (even lower than its fragment C-domain) by friction. The radius of gyration (R_g) of FL-mPrP in 0.5 mM AcOH obtained by SAXS was indeed significantly larger than the previously reported value that occurred at a high salt concentration (Figure 2). The fact that adding only 5 mM NaCl could largely increase the sedimentation coefficient of FL-mPrP from 1.32 ± 0.15 S to 1.72 ± 0.08 S, while the values hardly changed for the C-domain (from 1.55 ± 0.08 S to 1.6 ± 0.07 S) (Figure 3b) suggest that 5 mM salt is enough to induce the hydrophobic collapse of the flexible N-terminal polypeptide chain. The reduction of the ANS emitted fluorescence after the addition of salt also implied that FL-mPrP was more compact

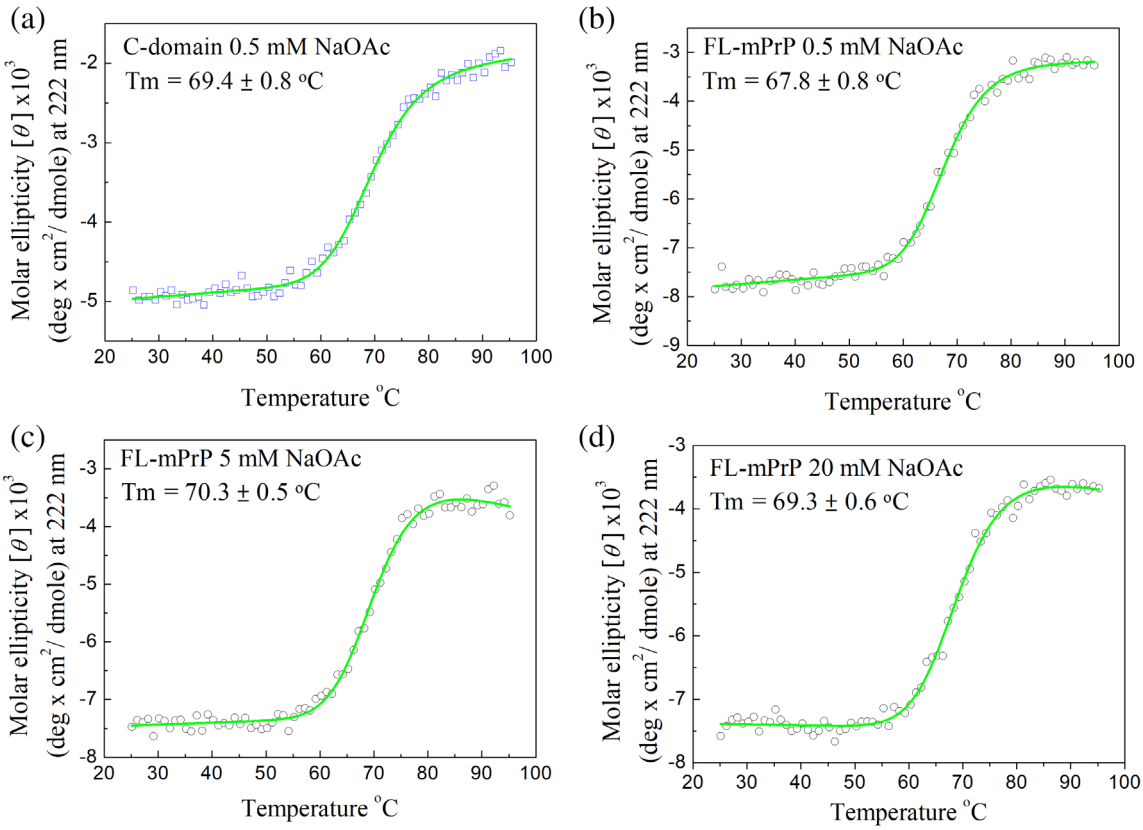

FIGURE 7 The thermal denaturation curves of the C-domain at 0.5 mM NaOAc (pH 5.2) (a) and FL-mPrP at various NaOAc concentrations (pH 5.2) (b–d). The melting temperature (T_m) of the sample is shown in each plot. FL-mPrP, full-length recombinant mouse prion protein

and that hydrophobic residues in the N-terminal part were buried (Figure 4). The 11 positive charges in the region of 23–99 hindered the structural collapse, probably due to charge repulsion. The charge-enhanced structural flexibility might be related to the ability of PrP^C to interact with other proteins, such as Aβ oligomers. To sum up, the PrP N-terminal region is disordered and does not have any secondary structure, but it is not an isolated polypeptide chain in the physiological condition, as depicted in many illustrations of prion protein structure.[39,40]

The melting temperatures of the C-domain and FL-mPrP were almost the same in 0.5 mM AcOH, which echoes the data reported by Moulick and Udgaonkar that moPrP(23–231) and moPrP(121–231) had the same stability against urea denaturation and thermal denaturation at pH 4.[41] They concluded that the N-terminal domain does not interact with the C-terminal domain (their C-terminal domain contains sequence 121–231) at pH 4. In our ANS-binding assay, our C-domain had a higher fluorescence intensity in the presence of 5 mM NaCl, indicating the C-domain had a more exposed hydrophobic surface (Figure 4). This is why the C-domain is prone to aggregation in the presence of salt. This aggregation propensity hampered the further study of the C-domain in the high salt condition. However, the exposed surface can be well shielded in the full-length protein by the presence of the N-domain. Based on our findings, we surmise that prion protein at pH 4 might look like a snowman with a fluffy head (Figure 9a), and the N-domain and the C-domain are the head and body, respectively. Many proteins, which are inclined to misfold and aggregate into amyloid fibrils, have an intrinsically disordered region, such as α-synuclein, TDP-43, tau, and prion protein.[42] The role of the unstructured region in protein aggregation is not clear yet and might depend on its location and distance with the interacting residues.[43,44] The protein/solvent interaction also affects the folding/aggregation behavior of proteins.[45] With the lack of hydrophobic residues, aggregation of intrinsically disordered proteins is affected by charge and lipophilicity of the solvent.[46] It has been reported that disordered regions could prevent peptide aggregation in a *cis* or *trans* manner, that is, to the other region of the same protein or to other peptides.[47,48] Proteins that could prevent protein aggregation are called chaperones. The intrinsically disordered N-domain serves like an intramolecular chaperone to protect the C-domain to minimize its possibility of interacting with the C-domain of other prion protein molecules, thereby potentially forming oligomeric,

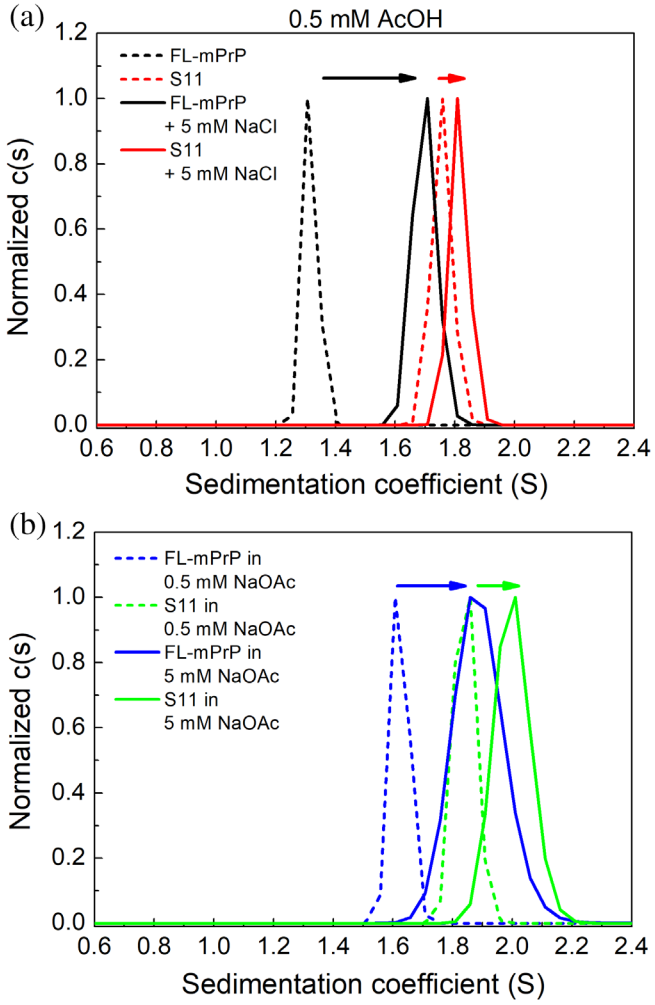

FIGURE 8 Comparison of the SV-AUC spectra of FL-mPrP and S11. (a) The proteins were dissolved in 0.5 mM AcOH with (solid line) or without (dashed line) adding 5 mM NaCl. Black: FL-mPrP; red: S11. (b) The proteins were dissolved in 0.5 mM NaOAc (dashed line) or 5 mM NaOAc (solid line). Blue: FL-mPrP; green: S11. The change upon salt increase is indicated by an arrow. AcOH, acetic acid; FL-mPrP, full-length recombinant mouse prion protein; SV-AUC, sedimentation velocity-analytical ultracentrifugation

prefibrillar species that could aggregate further to form amyloid fibrils. Because moPrP(121–231) is shorter and more soluble than our C-domain (sequence 106–230), the residues 106–120 are probably the segment that needs to be protected by the N-domain.

When the solution pH was 5.2, the thermal stability of FL-mPrP largely increased. The presence of the N-domain did not affect the structural stability of prion protein because there was no substantial difference in the melting temperatures of FL-mPrP and the C-domain (Figure 7). The stability enhancement at pH 5.2 might result from the glutamate-involved electrostatic interaction, such as between E200-K204-E207 and R208-E211 in the C-domain. Increasing the NaOAc concentration from 0.5 mM to 5 mM increased the sedimentation coefficient, but there was no change when the salt concentration was further increased to 20 mM NaOAc (Figure 6). The hydrodynamic radius of FL-mPrP estimated based on the sedimentation coefficient was 2.83–3.32 nm at pH 5.2, close to the radius of gyration measured by Carter et al. using SAXS at pH 5.1 (3.07 nm).[38] FL-mPrP has a bigger size at pH 4.2 than pH 5.2, suggesting that the structural collapse is related to the protonated/deprotonated state of glutamate. Because there are many positively charged residues but no glutamate in the N-domain, the N-domain might have electrostatic interactions with the glutamate residues in the C-domain. We surmise that the structure of FL-mPrP at pH 5.2 might look like a ball wrapped with a string (Figure 9a). Recently, McDonald et al. used a photoactivated cross-linker and mass analysis to examine the interdomain interactions of mouse prion protein at pH 7.4. They observed the interaction between the N-terminal polybasic 23–31 segment and the C-terminal 218–225 segment and the interactions between another N-terminal polybasic 99–108 segment and three C-terminal segments (155–162, 163–174, and 218–225).[49] The finding that mutating E199 to K significantly attenuated the interaction of the 99–108 segment with the C-terminal domain being consistent with our conclusion.

Unlike previous research, the way we dissect FL-mPrP into two domains, the N-domain (sequence 23–105) and the C-domain (106–230), is based on the structural integrity of FL-mPrP upon limited trypsin digestion. In the literature, researchers have commonly expressed and studied mPrP 89–230 or 120–230. Here, we studied mouse PrP 106–230 and observed significant aggregation effects; which suggest that the segment 106–120 is the source of protein aggregation and that the segment 89–105 might help to cover the hydrophobic patch. The 106–120 region consists of an important sequence divergent region in mammals (sequence TNLKHV, 106–111) followed by one hydrophobic, palindromic, and amyloidogenic sequence AGAAAAGA (112–119) (Figure 9b). The 89–105 region (sequence GQGGGTHNQWNKPSKPK) contains both hydrophobic and positively charged residues. As shown in Figure 4, salt-induced structural collapse exposed a hydrophobic surface in C-domain. N-domain contains many hydrophobic residues and positively charged residues. It can help the C-domain to bury the exposed hydrophobic surface during the structural collapse.

The human P102L, P105L/T/S, A117V, G131V, S132I, and A133V mutations and the truncated mutation Y145Stop result in Gerstman–Sträussler–Scheinker syndrome, and the G114V mutation results in familial Creutzfeldt–Jacob disease.[50–52] The hamster prion peptides haPrP106–128 and haPrP119–136 can effectively inhibit the cell-free conversion of prion protein from

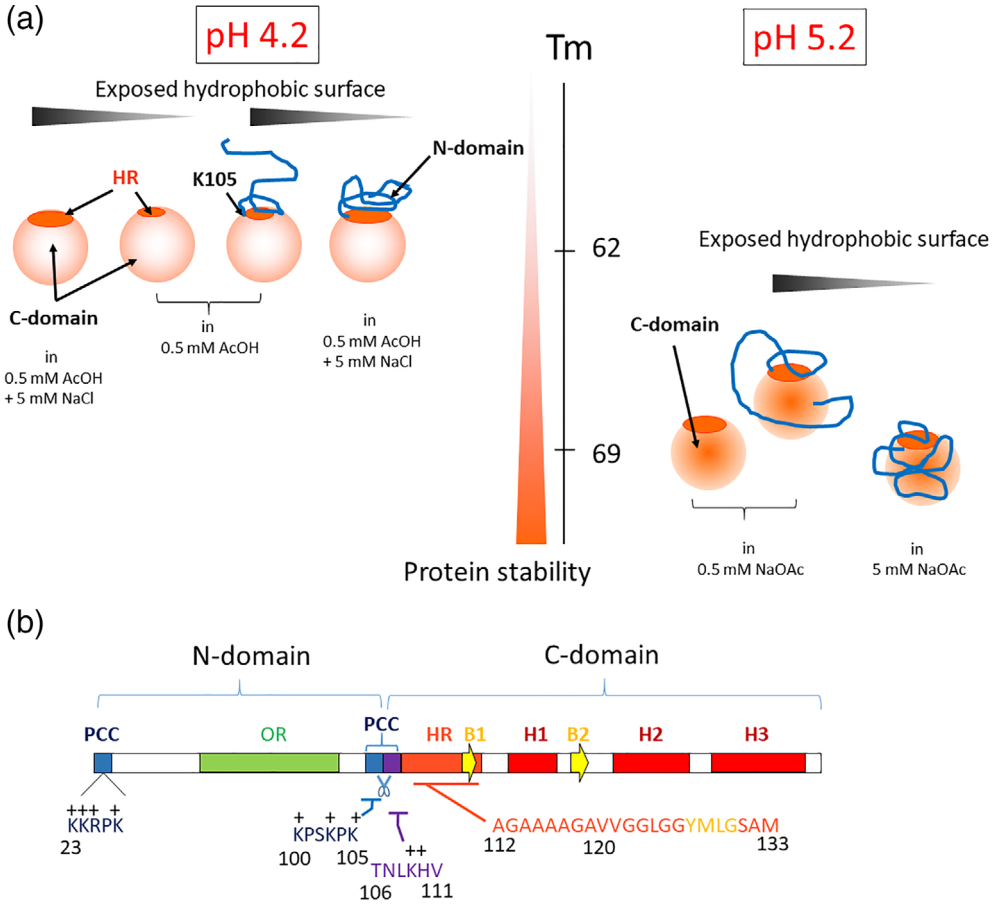

FIGURE 9 (a) Illustration of the condition-dependent structural collapse of mouse prion protein and its correlation with protein stability. The N-domain and the C-domain are displayed as a string and a ball, respectively. (b) Structural features of FL-mPrP: PCC, positively charged cluster; OR, octapeptide repeat; HR, hydrophobic region; B1 and B2, β-strand-1 and β-strand-2; H1–H3, α-helices 1, 2, and 3. The trypsin cutting site is between K105 and T106. The amino acid sequences of the positively charged cluster and hydrophobic region are listed (the residue numbers are shown below). FL-mPrP, full-length recombinant mouse prion protein

PrP^{sen} (protease-sensitive form) to PrP^{res} (protease-resistant form).[53,54] Lawson et al. reported that haPrPΔ34–113 altered PrP^{res} conformation, while did haPrPΔ34–94 not.[22] These data suggest that the region between the octarepeats and the first α-helix might affect either the structure of partially unfolded prion protein or the kinetics of prion conversion. Despite the fact that most structural studies did not find this region to be involved in the cross-β structure in the in vitro prepared prion fibrils,[4,5,8,10,55] some reports showed that this region is in the amyloid core of brain-derived PrP^{Sc} or in vitro prepared prion fibrils seeded by PrP^{Sc}.[6,9,12,56]

HaPrP106–126,[57] huPrP118–135, and huPrP105–132 have been reported to be neurotoxic.[58,59] The toxicity might be the result of the hydrophobic nature of the peptide in the interaction with cell membrane.[59] At physiological salt concentration and pH, the C-terminal globular domain might be wrapped and protected by the N-terminal disordered polypeptide chain. The interaction between the N-domain and the C-domain in PrP^{C} might be replaced by the interaction between the N-domain and the negatively charged lipid surface, such as POPS or POPG.[60] Morillas et al. have reported that the 23–145 region of huPrP23–231 interacted with lyso-PC/lyso-PS (2:1) liposomes and that this interaction decreased the thermostability of the protein, especially at acidic pH (pH 5).[60] This PrP–lipid interaction is pH dependent and stronger at lower pH, indicating the importance of the ionic interaction between the polybasic regions in the N-domain and lipid. It is known that prion conversion occurs in endosomes. When PrP^{C} is in the endosome, the pH drop not only releases the N-terminal chain from the C-terminal globular domain but also destabilizes the protein. It was reported that nucleic acid can destabilize the C-terminal domain at pH 5 but not at pH 7.[61] Of note, this destabilizing effect is again pH-dependent, just like the lipid. To sum up, the interaction between the N-terminal-disordered region and the C-terminal globular domain at neutral pH might prohibit the interaction between PrP and other destabilizing factors and have a protective role against prion conversion.

ACKNOWLEDGMENTS

AUC and CD spectroscopy were conducted in the Biophysical Instrumentation Laboratory at the Institute of Biological Chemistry, Academia Sinica. We acknowledge the use of the XL-A analytical ultracentrifuge in the Biophysics Core Facility, funded by Academia Sinica Core Facility and the Innovative Instrument Project AS-CFII108-111. We thank Cheng-Hsilin Hsieh for her technical assistance with the MALDI-TOF/TOF mass

spectrometry at the Genomics Core of the Institute of Molecular Biology. We also thank the DNA Sequencing Core Facility at the Institute of Biomedical Sciences, Academia Sinica for the DNA sequencing analysis. This core facility is funded by the Academia Sinica Core Facility and the Innovative Instrument Project (AS-CFII-108-115).

CONFLICT OF INTEREST

The authors declare no conflicts of interest.

AUTHOR CONTRIBUTIONS

Kuei-Ming Lin and Eric H.-L. Chen prepared the proteins and conducted most of the experiments; Jason C. Sang performed trypsin digestion and mass analysis; Meng-Ru Ho conducted AUC and the associated data analysis; Chih-Hsuan Lee prepared the mutant protein; Orion Shih, Chun-Jen Su, Yi-Qi Yeh, and U-Ser Jeng contributed to the SAXS experiment; and Eric H.-L. Chen and Rita P.-Y. Chen designed the experiments, analyzed the data, and wrote manuscript.

ORCID

Eric H.-L. Chen https://orcid.org/0000-0003-1641-5086
Rita P.-Y. Chen https://orcid.org/0000-0003-3987-033X

REFERENCES

1. Prusiner SB, Bolton DC, Groth DF, Bowman KA, Cochran SP, McKinley MP. Further purification and characterization of scrapie prions. Biochemistry. 1982;21:6942–6950.
2. Prusiner SB. Novel proteinaceous infectious particles cause scrapie. Science. 1982;216:136–144.
3. Riek R, Hornemann S, Wider G, Glockshuber R, Wuthrich K. NMR characterization of the full-length recombinant murine prion protein, mPrP(23-231). FEBS Lett. 1997;413:282–288.
4. Lu X, Wintrode PL, Surewicz WK. B-sheet core of human prion protein amyloid fibrils as determined by hydrogen/deuterium exchange. Proc Natl Acad Sci U S A. 2007;104:1510–1515.
5. Cobb NJ, Sonnichsen FD, McHaourab H, Surewicz WK. Molecular architecture of human prion protein amyloid: A parallel, in-register b-structure. Proc Natl Acad Sci U S A. 2007;104:18946–18951.
6. Smirnovas V, Kim JI, Lu X, Atarashi R, Caughey B, Surewicz WK. Distinct structures of scrapie prion protein (PrPSc)-seeded versus spontaneous recombinant prion protein fibrils revealed by hydrogen/deuterium exchange. J Biol Chem. 2009;284:24233–24241.
7. Wille H, Bian W, McDonald M, et al. Natural and synthetic prion structure from X-ray fiber diffraction. Proc Natl Acad Sci. 2009;106:16990–16995.
8. Tycko R, Savtchenko R, Ostapchenko VG, Makarava N, Baskakov IV. The alpha-helical C-terminal domain of full-length recombinant PrP converts to an in-register parallel beta-sheet structure in PrP fibrils: Evidence from solid state nuclear magnetic resonance. Biochemistry. 2010;49:9488–9497.
9. Smirnovas V, Baron GS, Offerdahl DK, Raymond GJ, Caughey B, Surewicz WK. Structural organization of brain-derived mammalian prions examined by hydrogen-deuterium exchange. Nat Struct Mol Biol. 2011;18:504–506.
10. Singh J, Udgaonkar JB. Dissection of conformational conversion events during prion amyloid fibril formation using hydrogen exchange and mass spectrometry. J Mol Biol. 2013;425:3510–3521.
11. Wang L-Q, Zhao K, Yuan H-Y, et al. Cryo-EM structure of an amyloid fibril formed by full-length human prion protein. Nat Struct Mol Biol. 2020;27:598–602.
12. Kraus A, Hoyt F, Schwartz CL, Hansen B, Hughson AG, et al. Structure of an infectious mammalian prion. bioRxiv. 2021. https://doi.org/10.1101/2021.02.14.431014.
13. Lauren J. Cellular prion protein as a therapeutic target in Alzheimer's disease. J Alzheimers Dis. 2014;38:227–244.
14. Purro SA, Nicoll AJ, Collinge J. Prion protein as a toxic acceptor of amyloid-beta oligomers. Biol Psychiatry. 2018;83:358–368.
15. Dohler F, Sepulveda-Falla D, Krasemann S, et al. High molecular mass assemblies of amyloid-β oligomers bind prion protein in patients with Alzheimer's disease. Brain. 2014;137:873–886.
16. Laurén J, Gimbel DA, Nygaard HB, Gilbert JW, Strittmatter SM. Cellular prion protein mediates impairment of synaptic plasticity by amyloid-β oligomers. Nature. 2009;457:1128–1132.
17. Chen S, Yadav SP, Surewicz WK. Interaction between human prion protein and amyloid-beta (Abeta) oligomers: Role of N-terminal residues. J Biol Chem. 2010;285:26377–26383.
18. Bueler H, Aguzzi A, Sailer A, Greiner RA, Autenried P, et al. Mice devoid of PrP are resistant to scrapie. Cell. 1993;73:1339–1347.
19. Fischer M, Rülicke T, Raeber A, et al. Prion protein (PrP) with amino-proximal deletions restoring susceptibility of PrP knockout mice to scrapie. EMBO J. 1996;15:1255–1264.
20. Flechsig E, Shmerling D, Hegyi I, et al. Prion protein devoid of the octapeptide repeat region restores susceptibility to scrapie in PrP knockout mice. Neuron. 2000;27:399–408.
21. Das NR, Miyata H, Hara H, et al. The N-terminal polybasic region of prion protein is crucial in prion pathogenesis independently of the octapeptide repeat region. Mol Neurobiol. 2020;57:1203–1216.
22. Lawson VA, Priola SA, Wehrly K, Chesebro B. N-terminal truncation of prion protein affects both formation and conformation of abnormal protease-resistant prion protein generated in vitro. J Biol Chem. 2001;276:35265–35271.
23. Shmerling D, Hegyi I, Fischer M, et al. Expression of amino-terminally truncated PrP in the mouse leading to ataxia and specific cerebellar lesions. Cell. 1998;93:203–214.
24. Baumann F, Tolnay M, Brabeck C, et al. Lethal recessive myelin toxicity of prion protein lacking its central domain. EMBO J. 2007;26:538–547.
25. Li A, Christensen HM, Stewart LR, Roth KA, Chiesa R, Harris DA. Neonatal lethality in transgenic mice expressing prion protein with a deletion of residues 105-125. EMBO J. 2007;26:548–558.
26. Linden R, Martins VR, Prado MAM, Cammarota M, Izquierdo I, Brentani RR. Physiology of the prion protein. Physiol Rev. 2008;88:673–728.
27. Christensen HM, Dikranian K, Li A, et al. A highly toxic cellular prion protein induces a novel, nonapoptotic form of neuronal death. Am J Pathol. 2010;176:2695–2706.
28. Li A, Barmada SJ, Roth KA, Harris DA. N-terminally deleted forms of the prion protein activate both Bax-dependent and

Bax-independent neurotoxic pathways. J Neurosci. 2007;27:852–859.
29. Liao Y-D, Jeng J-C, Wang C-F, Wang S-C, Chang S-T. Removal of N-terminal methionine from recombinant proteins by engineered *E. coli* methionine aminopeptidase. Prot Sci. 2004;13:1802–1810.
30. Dalbøge H, Bayne S, Pedersen J. In vivo processing of N-terminal methionine in *E. coli*. FEBS Lett. 1990;266:1–3.
31. Laue T, Shah B, Ridgeway T, Pelletier S. In: Harding SE, Horton HC, Rowe AJ, editors. Analytical ultracentrifugation in biochemistry & polymer science. London: Royal Society of Chemistry, 1992; p. 90–125.
32. Schuck P. Size-distribution analysis of macromolecules by sedimentation velocity ultracentrifugation and lamm equation modeling. Biophys J. 2000;78:1606–1619.
33. Yeh Y-Q, Liao K-F, Shih O, et al. Probing the acid-induced packing structure changes of the molten globule domains of a protein near equilibrium unfolding. J Phys Chem Lett. 2017;8:470–477.
34. Shih O, Yeh Y-Q, Liao K-F, et al. Membrane charging and swelling upon calcium adsorption as revealed by phospholipid nanodiscs. J Phys Chem Lett. 2018;9:4287–4293.
35. Rodriguez J, Gupta N, Smith RD, Pevzner PA. Does trypsin cut before proline? J Proteome Res. 2008;7:300–305.
36. Tria G, Mertens HD, Kachala M, Svergun DI. Advanced ensemble modelling of flexible macromolecules using X-ray solution scattering. IUCrJ. 2015;2:207–217.
37. Bernadó P, Mylonas E, Petoukhov MV, Blackledge M, Svergun DI. Structural characterization of flexible proteins using small-angle X-ray scattering. J Am Chem Soc. 2007;129:5656–5664.
38. Carter L, Kim SJ, Schneidman-Duhovny D, et al. Prion protein-antibody complexes characterized by chromatography-coupled small-angle X-ray scattering. Biophys J. 2015;109:793–805.
39. Legname G. Elucidating the function of the prion protein. PLoS Pathog. 2017;13:e1006458.
40. Ambadi Thody S, Mathew MK, Udgaonkar JB. Mechanism of aggregation and membrane interactions of mammalian prion protein. Biochim Biophys Acta Biomembr. 2018;1860:1927–1935.
41. Moulick R, Udgaonkar JB. Thermodynamic characterization of the unfolding of the prion protein. Biophys J. 2014;106:410–420.
42. Ross CA, Poirier MA. Protein aggregation and neurodegenerative disease. Nat Med. 2004;10(Suppl):S10–S17.
43. Hall D, Hirota N, Dobson CM. A toy model for predicting the rate of amyloid formation from unfolded protein. J Mol Biol. 2005;351:195–205.
44. Hall D, Hirota N. Multi-scale modelling of amyloid formation from unfolded proteins using a set of theory derived rate constants. Biophys Chem. 2009;140:122–128.
45. Abeln S, Frenkel D. Accounting for protein-solvent contacts facilitates design of nonaggregating lattice proteins. Biophys J. 2011;100:693–700.
46. Santos J, Iglesias V, Santos-Suárez J, et al. pH-dependent aggregation in intrinsically disordered proteins is determined by charge and lipophilicity. Cell. 2020;9:145.
47. Abeln S, Frenkel D. Disordered flanks prevent peptide aggregation. PLoS Comput Biol. 2008;4:e1000241.
48. Ikeda K, Suzuki S, Shigemitsu Y, et al. Presence of intrinsically disordered proteins can inhibit the nucleation phase of amyloid fibril formation of Aβ(1–42) in amino acid sequence independent manner. Sci Rep. 2020;10:12334.
49. McDonald AJ, Leon DR, Markham KA, Wu B, Heckendorf CF, et al. Altered domain structure of the prion protein caused by cu(2+) binding and functionally relevant mutations: analysis by cross-linking, MS/MS, and NMR. Structure. 2019;27:907–922.e905.
50. Mastrianni JA. The genetics of prion diseases. Genet Med. 2010;12:187–195.
51. Jeong B-H, Kim Y-S. Genetic studies in human prion diseases. J Korean Med Sci. 2014;29:623–632.
52. Lloyd SE, Mead S, Collinge J. Genetics of prion diseases. Curr Opin Genet Dev. 2013;23:345–351.
53. Chabry J, Caughey B, Chesebro B. Specific inhibition of in vitro formation of protease-resistant prion protein by synthetic peptides. J Biol Chem. 1998;273:13203–13207.
54. Chabry J, Priola SA, Wehrly K, Nishio J, Hope J, et al. Species-independent inhibition of abnormal prion protein (PrP) formation by a peptide containing a conserved PrP sequence. J Virol. 1999;73:6245–6250.
55. Nazabal A, Hornemann S, Aguzzi A, Zenobi R. Hydrogen/deuterium exchange mass spectrometry identifies two highly protected regions in recombinant full-length prion protein amyloid fibrils. J Mass Spectrom. 2009;44:965–977.
56. Groveman BR, Dolan MA, Taubner LM, Kraus A, Wickner RB, Caughey B. Parallel in-register intermolecular β-sheet architectures for prion-seeded prion protein (PrP) amyloids. J Biol Chem. 2014;289:24129–24142.
57. Ettaiche M, Pichot R, Vincent JP, Chabry J. In vivo cytotoxicity of the prion protein fragment 106-126. J Biol Chem. 2000;275:36487–36490.
58. Chabry J, Ratsimanohatra C, Sponne I, Elena P-P, Vincent J-P, Pillot T. In vivo and in vitro neurotoxicity of the human prion protein (PrP) fragment P118-135 independently of PrP expression. J Neurosci. 2003;23:462–469.
59. Haïk S, Peyrin JM, Lins L, Rosseneu MY, Brasseur R, et al. Neurotoxicity of the putative transmembrane domain of the prion protein. Neurobiol Dis. 2000;7:644–656.
60. Morillas M, Swietnicki W, Gambetti P, Surewicz WK. Membrane environment alters the conformational structure of the recombinant human prion protein. J Biol Chem. 1999;274:36859–36865.
61. Bera A, Nandi PK. Nucleic acid induced unfolding of recombinant prion protein globular fragment is pH dependent. Protein Sci. 2014;23:1780–1788.

SUPPORTING INFORMATION

Additional supporting information may be found online in the Supporting Information section at the end of this article.

How to cite this article: Chen EH-L, Lin K-M, Sang JC, Ho M-R, Lee C-H, Shih O, et al. Condition-dependent structural collapse in the intrinsically disordered N-terminal domain of prion protein. IUBMB Life. 2021;1–14. https://doi.org/10.1002/iub.2528